Transition Metal Chemistry
https://doi.org/10.1007/s11243-019-00363-x

Modification of porous lignin with metalloporphyrin as an efficient catalyst for the synthesis of cyclic carbonates

Kunpeng Song[1,3] · Cheng Tang[1] · Zhijuan Zou[1] · Yundang Wu[2]

Received: 13 September 2019 / Accepted: 28 October 2019

Abstract

The conversion of carbon dioxide into useful chemical raw materials is a necessary development for advancing carbon dioxide capture and storage technology. In this work, a Friedel–Crafts reaction of lignin and metalloporphyrin was used to produce a lignin-based porous organic polymer (P-(L-FeTPP)) with a surface area of up to 1153 $m^2\ g^{-1}$. P-(L-FeTPP)) efficiently catalyzed the cycloaddition reactions of epoxides and CO_2 under solvent-free conditions, with porphyrin iron acting as an active center. The product yield reached up to 99.6% after 12 h under 1 MPa CO_2 and 70 °C. A turnover number of 1481 was achieved, indicating that this catalyst is much more active than its homogeneous counterpart and is one of the most efficient lignin-supported heterogeneous catalysts ever reported. This method for the in situ incorporation of a metalloporphyrin into a lignin skeleton greatly improved the stability of the metal catalyst, and P-(L-FeTPP) was readily recycled and reused more than six times without any significant loss of catalytic activity. Thus, this catalyst design is promising for practical applications, including the industrial production of cyclic carbonates.

Introduction

As a major component of lignocellulosic materials, lignin accounts for a significant proportion of biomass (typically 15–40% of dried biomass), including wood and agricultural residues [1]. However, owing to its complex structure and a lack of effective degradation methods, lignin is currently burnt in significant quantities at source for heat and power, and its value has been far underestimated. In recent years, with increasing global interest in sustainable development and biomass-derived chemicals, strategies for the conversion of lignin into high value-added products have attracted wide attention [2]. The most economically valuable method is the conversion of lignin into small molecule aromatic monomers [3, 4]. Although there have been many reports in this regard, many challenges remain owing to the complexity of the lignin structure. Another strategy of interest is the modification of lignin to produce renewable composites for use as new sustainable fillers and functional materials [5–8].

Yang and colleagues used sulfomethylated lignin and polyaniline to prepare composite materials that enhanced the dispersion and conductivity of polyaniline in water [9]. Compared with pure ZnO, the lignin-based carbon–ZnO composite prepared by Wang et al. [10] exhibited greatly improved photocatalytic activity for the degradation of methyl orange and rhodamine B, illustrating the potential application of lignin-based composites in catalysis. Meng et al. [11] used organosolv lignin as a raw material to synthesize hypercross-linked polymers with high specific surface areas and rigid highly porous structures, which provided good CO_2 adsorption properties.

Carbon capture and storage technologies have evolved to include a wide variety of porous materials with excellent

---

Electronic supplementary material The online version of this article (https://doi.org/10.1007/s11243-019-00363-x) contains supplementary material, which is available to authorized users.

✉ Kunpeng Song
song19880405@126.com

✉ Yundang Wu
ydwu@soil.gd.cn

[1] Chemical Synthesis and Pollution Control Key Laboratory of Sichuan Province, College of Chemistry and Chemical Engineering, China West Normal University, Shida Road, Nanchong 637009, China

[2] Guangdong Key Laboratory of Integrated Agro-environmental Pollution Control and Management, Guangdong Institute of Eco-environmental Science and Technology, Guangzhou 510650, China

[3] Institute of Synthesis and Application of Functional Materials, China West Normal University, Nanchong 637009, China

capabilities for CO_2 selective adsorption [12]. However, as it is difficult to store CO_2 safely and permanently, converting it into valuable organic matter is an effective solution. The addition of CO_2 to epoxides to form cyclic carbonates represents one of the important reactions related to CO_2 transformation [13]. Various homogeneous organocatalysts and metal complexes have been developed for the catalytic cycloaddition of CO_2, including alkali metal salts, quaternary ammonium salts, Lewis acids, Schiff bases and metal porphyrins [14]. However, it is difficult to separate and reuse homogeneous catalysts. Furthermore, the purification of cyclic carbonates from a homogeneous reaction system is tedious and energy-consuming. To avoid these drawbacks and meet the needs of sustainable development, we envisaged the direct modification of inexpensive renewable lignin to produce a heterogeneous catalyst for the epoxide addition reactions of CO_2.

Metalloporphyrin complexes have broad application prospects in heterogeneous catalysis owing to their special biomimetic properties, and a large number of metalloporphyrins and their composites have been developed as heterogeneous catalysts [15–17]. Initially, metalloporphyrin oligomers, which show good optoelectronic properties and catalytic activity [18, 19], and conjugated metalloporphyrin polymers and porous organometallic porphyrin polymers [20, 21] were used as catalysts. Currently, immobilized active sites (metal porphyrin complexes) in networks of porous polymers tend to be used for heterogeneous catalysis [22]. For example, Kimoon and colleagues found that iron porphyrins embedded into a supramolecular porous organic cage effectively catalyzed the electrochemical reduction of CO_2 in water [23]. Although such materials often have good catalytic activities, they are not easy to synthesize. Conventional synthetic methods typically require the functionalization of small molecule precursors, and the available raw materials for such processes are limited [24]. Therefore, we attempted to incorporate a metalloporphyrin into a lignin skeleton using a simple external cross-linking method.

In this study, a metalloporphyrin-modified lignin polymer (P-(L-FeTPP)) was successfully synthesized via cross-linking using a Friedel–Crafts alkylation reaction [25], as described in Scheme 1. For comparison, we also prepared a Fe-supporting lignin-based polymer catalyst (P-(L-TPP)-Fe). Various techniques including Fourier transform infrared (FTIR) spectroscopy, thermogravimetric analysis (TGA), elemental analysis (EA), scanning electron microscopy (SEM), transmission electron microscopy (TEM) and X-ray photoelectron spectroscopy (XPS) were used to characterize the physicochemical properties of the catalysts. The experimental results suggested that P-(L-FeTPP), which exhibited a high surface area (1153 $m^2 g^{-1}$), was a superior catalyst for the transformation of CO_2 and epoxides into cyclic carbonates. This is the first example of the synthesis of cyclic carbonates using metalloporphyrin-modified lignin porous materials. A series of CO_2 cycloaddition experiments confirmed that the modification of lignin with a metalloporphyrin provided good catalytic activity and cyclability. Thus, this method for constructing efficient heterogeneous catalysts could afford a new opportunity for mitigating current CO_2 emissions.

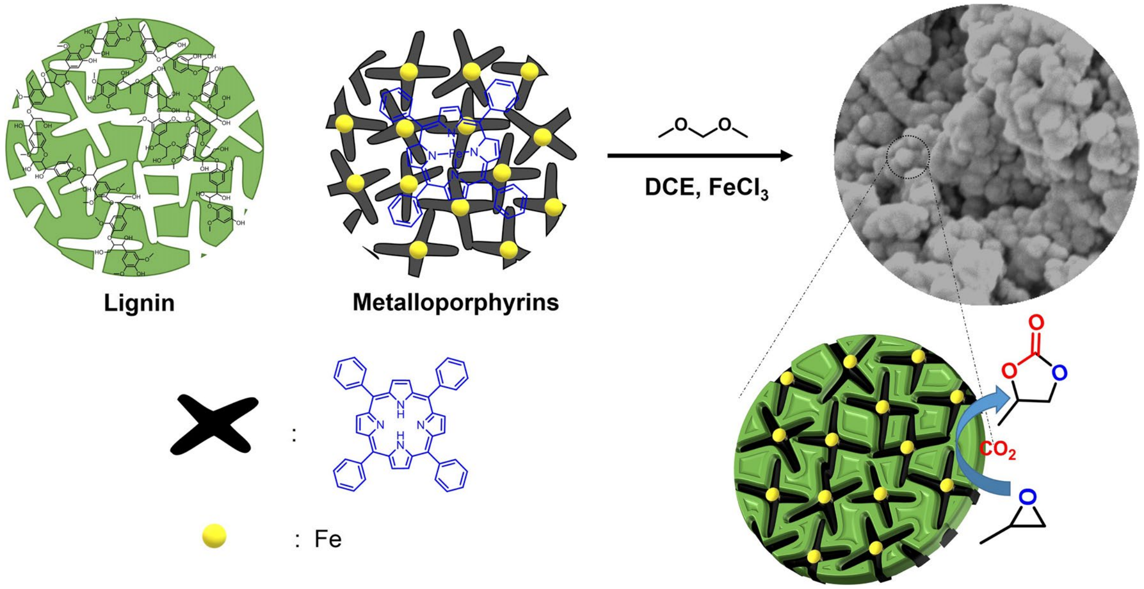

Scheme 1 Procedure for preparing P-(L-FeTPP)

Results and discussion

Catalyst characterization

Porphyrin-functionalized lignin was prepared from one-step bottom-up approach using the Friedel–Crafts alkylation cross-linking reaction between tetraphenylporphyrin and lignin following our previous report [26]. Initially, the chemical compositions of lignin (L), tetraphenylporphyrin (TPP), ferriporphyrin (FeTPP) and P-(L-FeTPP) were characterized using FTIR spectroscopy (Fig. 1a). The FTIR spectrum of FeTPP was almost identical to that of TPP. Both the P-(L-FeTPP) and FeTPP samples showed a characteristic vibrational peak at 1002 cm^{-1} corresponding to the pyrrole rings from Fe-porphyrins, confirming the presence of Fe-porphyrin moieties in the lignin-based porous polymer. Further, the series of bands near 1630–1690 cm^{-1} in the FTIR spectrum of P-(L-FeTPP) were assigned to the –C=N– stretching band.

The bands near 1250–950 cm^{-1} and 900–650 cm^{-1} were attributed to benzene skeleton stretching, C–H out-of-plane bending and in-plane bending vibrations of benzene. The obvious band near 2960–2920 cm^{-1} was assigned to the strong C–H stretching vibrations of methylene, which indicated the formation of methylene linkages. The above observations indicated that the metalloporphyrin-modified lignin-based porous polymer P-(L-FeTPP) was successfully synthesized. In addition, the UV–Vis spectra of FeTPP which are assigned based on the shift of the TPP spectrum indicate the successful complexation of iron in the porphyrin structure (Figure S1). The content of Fe was found to be 1.8 wt% using atomic absorption spectroscopy (AAS), and elemental mappings (Figure S2) showed that Fe atoms in the catalyst were always accompanied by nitrogen atoms (Table S1).

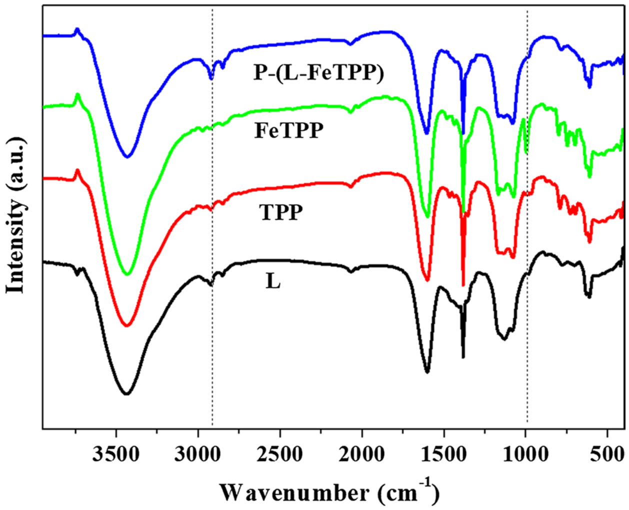

Fig. 1 FTIR spectra of lignin (L), tetraphenylporphyrin (TPP), ferriporphyrin (FeTPP) and the prepared catalyst (P-(L-FeTPP))

As observed by SEM, the P-(L-FeTPP) catalyst exhibited a rough surface morphology and numerous nanoparticles were observed (Fig. 2a, b) [27]; a porous surface structure in SEM images and the abundance of channel structures indicate that P-(L-FeTPP) has a high specific surface area. The high-resolution TEM images (Fig. 2c, d) also reveal the presence of microchannels. The TEM and SEM results suggest that the metalloporphyrin was uniformly grafted onto lignin.

For catalyst P-(L-TPP)-Fe, iron was supported via an impregnation method, so some of the iron was physically adsorbed and could not form M-N_4 structure; the adsorbed iron occupies microchannel and results differences in pore structure and specific surface area compared with P-(L-FeTPP). The nitrogen adsorption–desorption isotherms at 77 K for P-(L-FeTPP) and P-(L-TPP)-Fe are shown in Fig. 3a. The adsorption–desorption curves did not reveal a significant hysteresis loop and could be classified as Type-I isotherms according to IUPAC nomenclature. Furthermore, the curves rise rapidly under low relative pressures ($P/P_0 < 0.01$), indicating the existence of abundant micropores. The nonlocal density functional theory (NLDFT)-based pore size distributions of the modified lignin samples were obtained by combining the pore size distributions from N_2 adsorption at 77 K and CO_2 adsorption at 273 K (Fig. 3b, c). The pore distributions of P-(L-FeTPP) and P-(L-TPP)-Fe showed a dominant pore diameter centered at approximately 0.5 nm and 3.8 nm, respectively, and continuous mesoporous and microporous structures (Fig. 3b, c), which agreed with the shape of the nitrogen sorption isotherms and the TEM analysis. The total pore volumes of P-(L-FeTPP) and P-(L-TPP)-Fe were 0.66 and 0.69 $cm^3\ g^{-1}$, respectively, whereas the BET-specific surface areas of these catalysts, calculated from the N_2 isotherms at 77 K, were similar (1153 and 1148 $m^2\ g^{-1}$, respectively). As the micropore surface area of P-(L-FeTPP) was larger than that of P-(L-TPP)-Fe (Table 1), we hypothesize that some of the supported Fe was taken up in the micropores of P-(L-TPP)-Fe.

Catalytic performance in CO_2 cycloaddition reactions

The catalytic performance of the modified lignin polymer was investigated for the CO_2 cycloaddition reaction with propylene oxide (PO) as a model reaction under co-catalyst conditions. First, we examined the activity of P-(L-FeTPP) and P-(L-TPP)-Fe. As shown in Table 1, with an iron load of 1.8 wt%, P-(L-FeTPP) gave a 99.6% yield (Table 2, entry 6), showing an obvious advantage over P-(L-TPP)-Fe with an iron load of 9.8 wt% (90.0% yield, Table 2, entry 7). This result illustrates the high efficiency of the active center

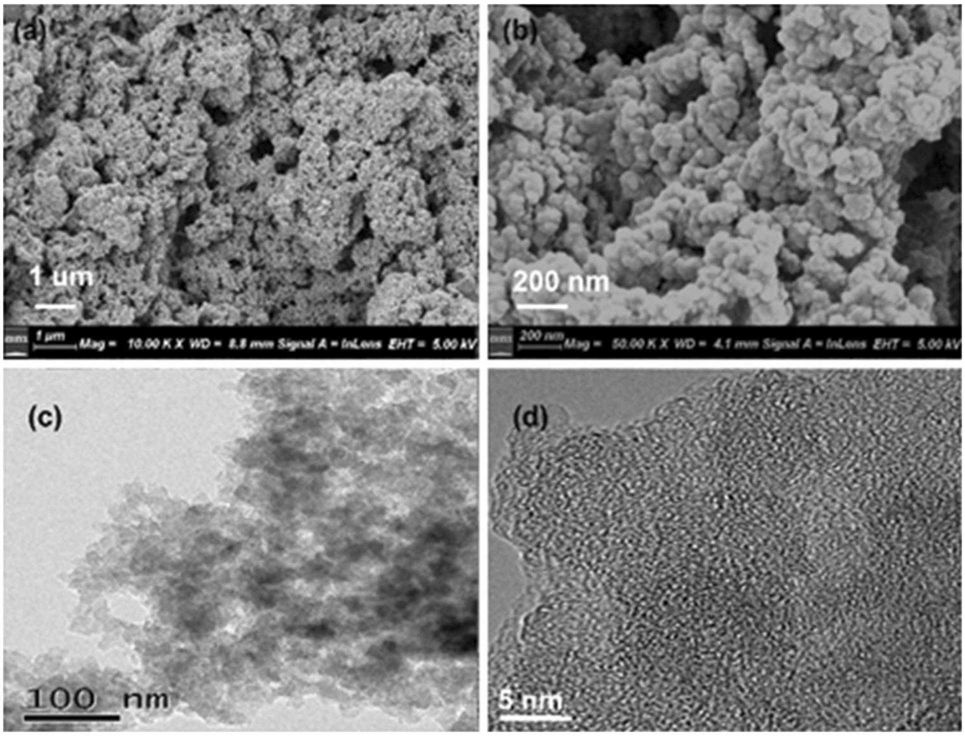

Fig. 2 SEM (**a**, **b**) and TEM (**c**, **d**) images of P-(L-FeTPP)

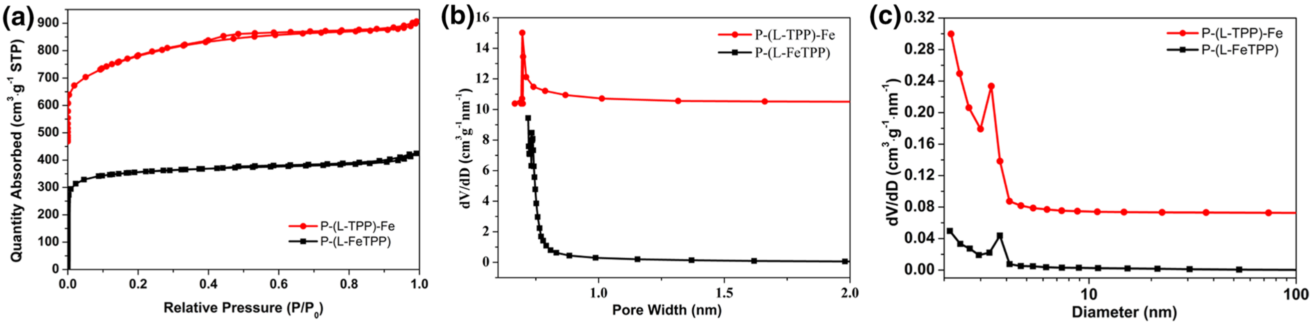

Fig. 3 N_2 adsorption–desorption isotherms at 77 K (**a**) and pore size distributions (**b**, **c**) of P-(L-FeTPP) and P-(L-TPP)-Fe

Table 1 Pore textural properties of P-(L-FeTPP) and P-(L-TPP)-Fe

Catalyst	S^{a}_{BET} ($m^2\ g^{-1}$)	S^{b}_{Micro} ($m^2\ g^{-1}$)	V^{c}_{Total} ($cm^3\ g^{-1}$)	V^{d}_{Micro} ($cm^3\ g^{-1}$)	S_{Micro}/S_{BET} (%)	V_{Micro}/V_{Total} (%)	Fe^{e} (wt%)
P-(L-FeTPP)	1153	944	0.66	0.46	81.9	69.7	1.8
P-(L-TPP)-Fe	1148	289	0.69	0.11	25.2	15.9	9.8

[a] Surface area calculated from the N_2 adsorption isotherm in the relative pressure (P/P_0) range of 0.08–0.22

[b] Micropore surface area calculated from the N_2 adsorption isotherm using the t-plot method based on the Harkins–Jura equation

[c] Total pore volume at $P/P_0 = 0.9916$

[d] Micropore volume derived from the t-plot method; [e] metal content detected by AAS

in P-(L-FeTPP). Table 2 summarizes the performance of various catalytic systems. No product was detected without catalyst (Table 2, entry 1), and a yield of only 10.6% was obtained after 12 h when P-(L-FeTPP) was used without the co-catalyst tetrabutylammonium bromide (TBAB) (Table 2, entry 5). Moreover, the PO/CO_2 coupling reaction

Table 2 Results of the cycloaddition reaction of CO_2 with PO using various catalysts

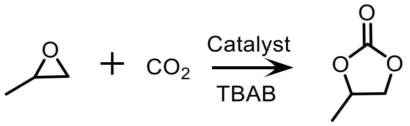

Entry	Catalyst	TBAB (mmol)	*T* (°C)	*t* (h)	Yield (%)
1	None	0	70	12	0
2	None	1.8	70	12	22.3
3	L	1.8	70	12	31.2
4	FeTPP	1.8	70	12	48.0
5	P-(L-FeTPP)	0	70	12	10.6
6	P-(L-FeTPP)	1.8	70	12	99.6
7	P-(L-TPP)-Fe	1.8	70	12	90.0
8	P-(L-FeTPP)	1.8	25	48	99.0

Reaction conditions: 20 mmol epoxide, 40 mg catalyst, 1 MPa CO_2, yields determined by GC using mesitylene as an internal standard

catalyzed by the co-catalyst TBAB only gave a 22.3% yield in the absence of P-(L-FeTPP) (Table 2, entry 2). However, combining P-(L-FeTPP) or P-(L-TPP)-Fe with TBAB as a co-catalyst enhanced the yield of the coupling reaction catalyzed to 99.6% and 90.0%, respectively (Table 2, entries 6 and 7). This result is notably better than the 48.0% and 31.2% yields obtained when the co-catalysts were used with FeTPP and lignin, respectively (Table 2, entries 3 and 4). Moreover, when the reaction was conducted at room temperature, P-(L-FeTPP) gave a 99% yield after 48 h (Table 2, entry 8). Therefore, we believe that the excellent catalytic performance of P-(L-FeTPP) can be ascribed to strong interactions between iron porphyrin and the lignin polymer skeleton as well as the concentration of CO_2 near the catalytic sites located in the highly porous structure.

Compared with other catalyst systems, P-(L-FeTPP) shows high turnover numbers (TONs) and yields under ambient conditions (Table S2) and was superior in terms of reaction temperature, CO_2 pressure and reaction time. Although some previous catalytic systems have been reported to have higher turnover frequencies (TOFs) [28] than this system, from these results, we can conclude that P-(L-FeTPP) is one of the most efficient catalysts for the chemical conversion of CO_2 into cyclic carbonates at room temperature and atmospheric pressure.

To confirm the composition of the as-obtained samples and the chemical states of the heteroatom, XPS characterization was performed (Fig. 4). As shown in Fig. 4b, deconvolution of the N 1 s signal in P-(L-TPP)-Fe reveals three types of nitrogen species: pyridinic N (398.7 eV), quaternary N (400.6 eV) and oxidized N (402.6 eV). However, the deconvoluted signal for P-(L-FeTPP) only reveals pyridinic N (398.6 eV) and quaternary N (400.4 eV). The in situ construction of FeTPP in the lignin skeleton likely induces the decomposition and reconstruction of N species, resulting in the disappearance of oxidized N (402.6 eV) [29]. Pyridinic N corresponds to N atoms doped at the edges of the graphitic carbon layers, whereas quaternary N corresponds to doping within the graphitic carbon plane. It has been reported that quaternary N can enhance the electric transmission performance, whereas pyridinic N may provide active sites that enhance metal anchoring and effectively avoid agglomeration, which further improves the catalytic activity and stability of metal catalysts [30, 31]. Hence, all the N species in P-(L-FeTPP) are expected to play a crucial role in the reaction process, but the contribution of oxidized N in P-(L-TPP)-Fe is uncertain. As shown by the high-resolution Fe 2p XPS spectrum (Fig. 4a), the binding energies of the main spin–orbit doublet (Fe $2p_{1/2}$ and Fe $2p_{3/2}$) for the P-(L-FeTPP) catalyst appear at 723.7 and 711.5 eV with a spin–orbital doublet splitting ($\Delta = \text{Fe } 2p_{1/2} - \text{Fe } 2p_{3/2}$) of 12.1 eV. These binding energies are higher than the standard values [32], revealing that strong interactions between FeTPP and lignin-based polymer decrease the electron density on the Fe atom. In comparison, a slight shift (~0.3 eV) of the Fe 2p peaks is observed for P-(L-TPP)-Fe, indicating that additional electronic interactions occur between Fe and N species in the polymer skeleton. The additional doublet at

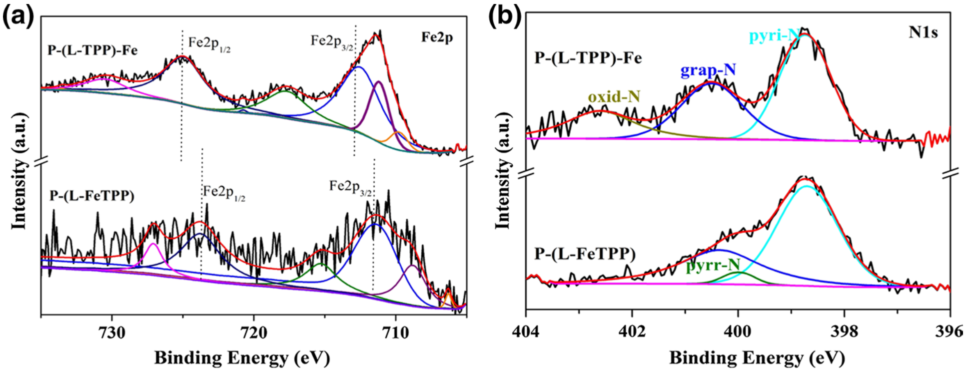

Fig. 4 High-resolution Fe 2p (**a**) and N 1 s (**b**) XPS spectra of P-(L-FeTPP) and P-(L-TPP)-Fe

approximately 727.0 and 715.4 eV is attributed to a higher oxidation state of Fe, suggesting the formation of Fe–O or Fe–N bonds. As the formation of Fe–O bonds is less likely in the present synthesis, this higher oxidation state is mainly attributed to the formation of Fe–N bonds.

Substrate scope of the P-(L-FeTPP)-catalyzed CO_2 cycloaddition reaction

To examine the scope of the P-(L-FeTPP) catalyst, CO_2 cycloaddition reactions were performed with a variety of substituted epoxides, as summarized in Table 3. Generally, a low loading of P-(L-FeTPP) (1.8 wt%, 40 mg) with co-catalyst TBAB (1.8 mmol) was used to catalyze the reaction at 70 °C and 1 MPa CO_2. PO (Table 3, entry 1) and 1-butene oxide (Table 3, entry 2) gave cyclic carbonates in 99.6% and 99.0% yield, respectively, in 24 h. Epibromohydrin, epichlorohydrin and 1,2-epoxyethylbenzene were also transformed into cyclic carbonates with high efficiency (Table 3, entries 3–5). However, glycidyl phenyl ether displayed a comparatively low selectivity and a complex mixture of solids was formed after 6 h of reaction (Table 3, entry 6), which is most probably a result of the steric hindrance and electronic effects [33] of the glycidyl phenyl ether.

Stability and regeneration

As recovery and reuse are very important factors when evaluating the performance and practical applications of a catalyst, we also investigated the recyclability of P-(L-FeTPP). Using simple centrifugation, the porous catalyst can be simply recovered and reused at least five times, with recovered P-(L-FeTPP) showing nearly the same reactivity as the original catalyst (Fig. 5). In addition, an AAS analysis of the recovered catalyst after the fifth run revealed a Fe content of 1.6 wt%, which is nearly the same as the content

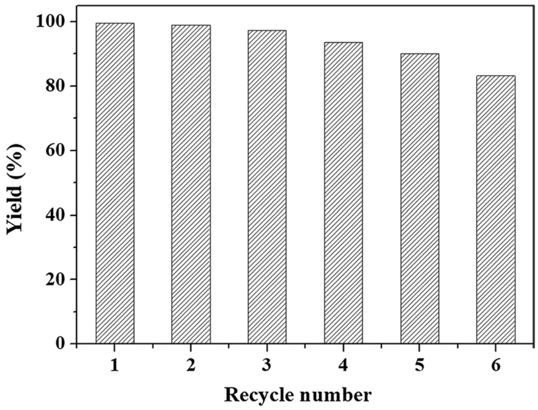

Fig. 5 Recyclability of P-(L-FeTPP) for the chemical conversion of CO_2 and PO under solvent-free conditions

Table 3 Coupling of various substituted epoxides with CO_2 catalyzed by P-(L-FeTPP)

Entry	Epoxide	Product	Time (h)	Yield (%)
1		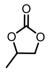	12	99.6
2	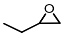	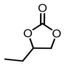	12	99
3	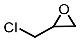	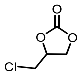	12	77.3
4	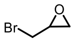	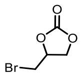	12	86.1
5	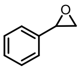	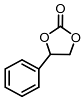	12	88.1
6	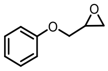	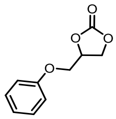	36	-

Reaction conditions: 20 mmol epoxide, 40 mg catalyst, 1 MPa CO_2, yields determined by GC using mesitylene as an internal standard of the fresh sample (1.8 wt%). In addition, the P-(L-FeTPP) was highly stable in air, as no obvious decrease in activity was observed after exposure of the catalyst to air for several days.

Conclusions

In summary, a novel lignin-based catalyst P-(L-FeTPP) with a surface area of up to 1148 $m^2\ g^{-1}$ was prepared by modification of lignin with metalloporphyrin moieties. With the co-catalyst TBAB, P-(L-FeTPP) exhibited high catalytic activity, high selectivity and good recyclability for the cycloaddition of CO_2 and epoxides to produce cyclic carbonates. The results indicated that the high catalytic activity of P-(L-FeTPP) originated from the strong interaction between the metal and the ligand, with the lignin polymer skeleton providing a large amount of reaction sites. This synthetic strategy for multifunctional lignin materials can potentially be applied to design other modified lignins for highly efficient catalytic processes. We believe that our results will inspire further developments of functional porous organic polymer materials for CO_2 conversion.

Experimental

Materials

Benzaldehyde, pyrrole (distilled), propionic acid, TBAB, benzene, dimethoxymethane (FDA) and 1,2-dichloroethane (DCE) were purchased from Aladdin Chemical Reagent Co. Ltd. Ferric chloride anhydrous, alkaline lignin (L), 1,3,5-trimethylbenzene and other solvents were purchased from Adamas-Beta. All compounds are analytically pure and were used without further purification.

Preparation of metalloporphyrin-modified lignin polymers

Synthesis of TPP

TPP was synthesized by a literature method [34]. Briefly, 30 mL of propionic acid was added to a 100-mL three-necked flask, condensed and refluxed at 125 °C. Benzaldehyde (0.9 g, 8.48 mmol) and freshly distilled pyrrole (0.5703 g, 8.5 mmol) were dispersed in 5 mL of propionic acid and ultrasonicated for 5 min (the color of the mixture gradually changed from dark green to purple). Then, the mixture was added dropwise to the above prepared propionic acid, stirring vigorously for 5 h. After completion of the reaction, 20 mL of ethanol was added, and the mixture was allowed to stand overnight, suction filtered, washed with a large amount of ethanol until colorless and dried in a vacuum oven at 100 °C. Yield: 29%. ^1H NMR (400 MHz, $CDCl_3$) $\delta -2.70$ (*s*, 2H, N–H), 8.90 (*s*, 8H, pyrrole-H), 8.27 (*d*, $J = 7.5$ Hz, 8H), 7.78–7.76 (*m*, 12H) (Figure S3).

Synthesis of FeTPP

A 50-mL two-necked round-bottomed flask was charged with a solution of TPP (0.3 g, 0.488 mmol) in dimethylformamide (DMF, 10 mL). Then, a solution of $FeCl_3$ (0.78 g, 4.88 mmol) in DMF (5 mL) was added in portions and the mixture was refluxed for 5 h. After completion of the reaction, 20 mL of deionized water was added and the mixture was allowed to stand overnight, suction filtered, washed with a large amount of ethanol and deionized water until colorless, and dried in a vacuum oven at 100 °C.

Synthesis of P-(L-FeTPP)

In a typical method, FeTPP (0.325 mmol, 0.2 g), alkaline lignin (0.2 g) and benzene (1.3 mmol, 0.1014 g) were dissolved in DCE (5 mL). After complete dissolution of the substrate, FDA (4 mmol, 0.304 g) and anhydrous $FeCl_3$ (12 mmol, 1.95 g) were added at room temperature. The resulting mixture was heated at 45 °C for 5 h and 80 °C for 19 h to complete the condensation reaction and obtain a porous structure. The resulting solid product was washed with methanol several times until the filtrate liquor was nearly colorless, and then, the product was subjected to Soxhlet extraction in methanol and DCM for 48 h followed by drying in a vacuum oven at 60 °C for 12 h. The catalyst was obtained as a dark colored powder.

Synthesis of P-(L-TPP)-Fe

In a typical method, TPP (0.325 mmol, 0.2 g), alkaline lignin (0.2 g) and benzene (1.3 mmol, 0.1014 g) were dissolved in DCE (5 mL). After complete dissolution of the substrate, FDA (4 mmol, 0.304 g) and anhydrous $FeCl_3$ (12 mmol, 1.95 g) were added at room temperature. The resulting mixture was heated at 45 °C for 5 h and 80 °C for 19 h to complete the condensation reaction and obtain a porous structure. The resulting solid product was washed with methanol several times until the filtrate liquor was nearly colorless, and then, the product was subjected to Soxhlet extraction in methanol and DCM for 48 h followed by drying in a vacuum oven at 60 °C for 12 h. The catalyst was obtained as a dark colored powder and denoted as P-(L-TPP).

A 100-mL round-bottomed flask was charged with a solution of L-TPP (0.3 g) in 30 mL of methanol and stirred for 4 h. Then, 0.087 g of $FeCl_3$ dispersed in 5 mL of methanol was added dropwise and the resulting mixture was stirred for

20 h. Subsequently, the methanol was evaporated to obtain P-(L-TPP)-Fe.

Catalyst characterization

FTIR spectra of the samples were obtained under ambient conditions at a resolution of 4 cm^{-1} in the wavenumber range of 4000–400 cm^{-1} using a NEX-US670 spectrometer. C, H and N EAs were performed on a Vario EL cube instrument. TGA was carried out using a NETZSCH STA 449 F3 instrument by heating samples from 40 to 800 °C at a heating rate of 10 °C min^{-1} under an air atmosphere. Solution ^{1}H NMR data were collected using a Varian INOVA 500NB spectrometer using TMS as an internal standard. SEM images were obtained using a GeminiSEM 500 scanning electron microscope. TEM images were obtained using a JEM-2100F field emission electron microscope (JEOL, Japan), which incorporated a probe corrector, at an acceleration voltage of 200 kV. The N_2 adsorption and desorption measurements were performed on a Quantachrome ASIQM0000-5 analyzer at 77 K. Specific surface areas (S_{BET}) were calculated using the Brunauer–Emmett–Teller (BET) method, and the pore size distributions were determined using NLDFT. XPS analysis was carried out on an ESCALAB 250 spectrometer. Metal contents were analyzed by atomic absorption spectrometry (AAS) on a PerkinElmer AA-300. Gas chromatography (GC) analysis was performed on an Agilent Technologies 7890A gas chromatograph equipped with a flame ionization detector and a capillary column (Rtx-5, 30 m × 0.32 mm × 0.25 μm).

Typical procedure for the cycloaddition of epoxides with CO_2

The catalytic performance of the catalyst was investigated by using the cycloaddition of CO_2 and PO as a model reaction. All the cycloaddition reactions were conducted in a 25-mL stainless steel autoclave operated in semi-batch mode (CO_2 was supplied to the reactor once) unless indicated otherwise. Typically, the epoxide, TBAB, and the catalyst were quickly added into the autoclave. After sealing and purging with CO_2 three times, the autoclave was pressurized with CO_2 to the required pressure, followed by stirring at the required temperature. After the appropriate reaction time, the autoclave was cooled to 0 °C and excess CO_2 was released slowly. Subsequently, the reaction mixture was extracted with ethyl acetate (3 × 2 mL), and the product yields and selectivity were determined by GC analysis using the internal standard method. The purities and structures of the products were also confirmed by GC–MS analysis. The catalyst was recycled by filtering, washing and drying and then used for the next run without further purification.

Acknowledgements This work was financially supported by the National Natural Science Foundations of China (41701305), the Science and Technology Planning Project of Guangdong Province (2017B030314092), Science and Technology Foundation of Sichuan Province (2017JY0015), the Fundamental Research Funds of CWNU (17C038) and the Meritocracy Research Funds of CWNU (17Y031).

References

1. Supanchaiyamat N, Jetsrisuparb K, Knijnenburg JTN, Tsang DCW, Hunt AJ (2019) Lignin materials for adsorption: current trend, perspectives and opportunities. Bioresour Technol 272:570
2. Sun Z, Fridrich B, De Santi A, Elangovan S, Barta K (2018) Bright side of lignin depolymerization: toward new platform chemicals. Chem Rev 118:614
3. Riaz A, Verma D, Zeb H, Lee JH, Kim JC, Kwak SK, Kim J (2018) Solvothermal liquefaction of alkali lignin to obtain a high yield of aromatic monomers while suppressing solvent consumption. Green Chem 20:4957
4. Ojha DK, Viju D, Vinu R (2017) Fast pyrolysis kinetics of alkali lignin: evaluation of apparent rate parameters and product time evolution. Bioresour Technol 241:142
5. Mohanty Amar K, Vivekanandhan Singaravelu, Pin Jean-Mathieu, Misra M (2018) Composites from renewable and sustainable resources: challenges and innovations. Science 362:536
6. Ma Y, Dai J, Wu L, Fang G, Guo Z (2017) Enhanced anti-ultraviolet, anti-fouling and anti-bacterial polyelectrolyte membrane of polystyrene grafted with trimethyl quaternary ammonium salt modified lignin. Polymer 114:113
7. Ji T, Chen L, Schmitz M, Bao FS, Zhu J (2015) Hierarchical macrotube/mesopore carbon decorated with mono-dispersed Ag nanoparticles as a highly active catalyst. Green Chem 17:2515
8. Li Z, Chen J, Ge Y (2017) Removal of lead ion and oil droplet from aqueous solution by lignin-grafted carbon nanotubes. Chem Eng J 308:809
9. Yang D, Huang W, Qiu X, Lou H, Qian Y (2017) Modifying sulfomethylated alkali lignin by horseradish peroxidase to improve the dispersibility and conductivity of polyaniline. Appl Surf Sci 426:287
10. Wang H, Qiu X, Liu W, Yang D (2017) Facile preparation of well-combined lignin-based carbon/ZnO hybrid composite with excellent photocatalytic activity. Appl Surf Sci 426:206
11. Meng QB, Weber J (2014) Lignin-based microporous materials as selective adsorbents for carbon dioxide separation. Chemsuschem 7:3312
12. Xu S, He J, Jin S, Tan B (2018) Heteroatom-rich porous organic polymers constructed by benzoxazine linkage with high carbon dioxide adsorption affinity. J Colloid Interface Sci 509:457
13. Martín C, Fiorani G, Kleij AW (2015) Recent advances in the catalytic preparation of cyclic organic carbonates. ACS Catal 5:1353
14. Saptal Vitthal, Shinde Digambar Balaji, Banerjee R, Bhanage BM (2016) State-of-the-Art catechol porphyrin COF catalyst for chemical fixation of carbon dioxide via cyclic carbonates and oxazolidinones. Catal Sci Technol 6:6152
15. Romelt C, Song J, Tarrago M, Rees JA, Van Gastel M, Weyhermuller T, Debeer S, Bill E, Neese F, Ye S (2017) Electronic structure of a formal iron(0) porphyrin complex relevant to CO_2 reduction. Inorg Chem 56:4746
16. Wang S, Song K, Zhang C, Shu Y, Li T, Tan B (2017) A novel metalporphyrin-based microporous organic polymer with high CO_2 uptake and efficient chemical conversion of CO_2 under ambient conditions. J Mater Chem A 5:1509

17. Bai D, Duan S, Hai L, Jing H (2012) Carbon dioxide fixation by cycloaddition with epoxides, catalyzed by biomimetic metalloporphyrins. ChemCatChem 4:1752
18. Kim MH, Song T, Seo UR, Park JE, Cho K, Lee SM, Kim HJ, Ko Y-J, Chung YK, Son SU (2017) Hollow and microporous catalysts bearing Cr(iii)–F porphyrins for room temperature CO_2 fixation to cyclic carbonates. J Mater Chem A 5:23612
19. Sigen A, Zhang Y, Li Z, Xia H, Xue M, Liu X, Mu Y (2014) Highly efficient and reversible iodine capture using a metalloporphyrin-based conjugated microporous polymer. Chem Commun 50:8495
20. Dai Z, Sun Q, Liu X, Bian C, Wu Q, Pan S, Wang L, Meng X, Deng F, Xiao F-S (2016) Metalated porous porphyrin polymers as efficient heterogeneous catalysts for cycloaddition of epoxides with CO_2 under ambient conditions. J Catal 338:202
21. Chen Y, Luo R, Xu Q, Zhang W, Zhou X, Ji H (2017) State-of-the-art aluminum porphyrin-based heterogeneous catalysts for the chemical fixation of CO_2 into cyclic carbonates at ambient conditions. ChemCatChem 9:767
22. Yuan K, Song T, Wang D, Zhang X, Gao X, Zou Y, Dong H, Tang Z, Hu W (2018) Effective and selective catalysts for cinnamaldehyde hydrogenation: hydrophobic hybrids of metal-organic frameworks, metal nanoparticles, and micro- and mesoporous polymers. Angew Chem Int Ed 57:5708
23. Smith PT, Benke BP, Cao Z, Kim Y, Nichols EM, Kim K, Chang CJ (2018) Iron porphyrins embedded into a supramolecular porous organic cage for electrochemical CO_2 reduction in water. Angew Chem Int Ed 57:9684
24. Liu X, Tang B, Long J, Zhang W, Liu X, Mirza Z (2018) The development of MOFs-based nanomaterials in heterogeneous organocatalysis. Sci Bull 63:502
25. Tang C, Zou Z, Fu Y, Song K (2018) Highly dispersed DPPF locked in knitting hyper-crosslinked polymers as efficient and recyclable catalyst. ChemistrySelect 3:5987
26. Fu Y-F, Song K-P, Zou Z-J, Li M-Q (2018) External cross-linked sulfonate-functionalized N-heterocyclic carbenes: an efficient and recyclable catalyst for Suzuki–Miyaura reactions in water. Transition Met Chem 43:665
27. Hou S, Razzaque S, Tan B (2019) Effects of synthesis methodology on microporous organic hyper-cross-linked polymers with respect to structural porosity, gas uptake performance and fluorescence properties. Polym Chem 10:1299
28. Ema T, Miyazaki Y, Shimonishi J, Maeda C, Hasegawa J-Y (2014) Bifunctional porphyrin catalysts for the synthesis of cyclic carbonates from epoxides and CO_2: structural optimization and mechanistic study. J Am Chem Soc 136:15270
29. Gottfried JM, Flechtner K, Kretschmann A, Lukasczyk T, Steinrück H-P (2006) Direct synthesis of a metalloporphyrin complex on a surface. J Am Chem Soc 128:5644
30. Song K, Zou Z, Wang D, Tan B, Wang J, Chen J, Li T (2016) Microporous organic polymers derived microporous carbon supported Pd catalysts for oxygen reduction reaction: impact of framework and heteroatom. J Phys Chem C 120:2187
31. Li S, Wu D, Cheng C, Wang J, Zhang F, Su Y, Feng X (2013) Polyaniline-coupled multifunctional 2D metal oxide/hydroxide graphene nanohybrids. Angew Chem Int Ed 52:12105
32. Deng F, Garcia-Rodriguez O, Olvera-Vargas H, Qiu S, Lefebvre O, Yang J (2018) Iron-foam as a heterogeneous catalyst in the presence of tripolyphosphate electrolyte for improving electro-Fenton oxidation capability. Electrochim Acta 272:176
33. Jiménez-Gómez CP, Cecilia JA, García-Sancho C, Moreno-Tost R, Maireles-Torres P (2019) Selective production of furan from gas-phase furfural decarbonylation on Ni-MgO catalysts. ACS Sustain Chem Eng 7:7676
34. Adler AD, Longo FR, Finarelli JD, Goldmacher J (1967) A simplified synthesis for meso-tetraphenylporphin. J Org Chem 32:476